Japanese Journal of Applied Physics **56**, 06HA02 (2017)
https://doi.org/10.7567/JJAP.56.06HA02

PROGRESS REVIEW

Progress and prospects in nanoscale dry processes: How can we control atomic layer reactions?

Kenji Ishikawa[1*], Kazuhiro Karahashi[2], Takanori Ichiki[3], Jane P. Chang[4], Steven M. George[5], W. M. M. Kessels[6], Hae June Lee[7], Stefan Tinck[8], Jung Hwan Um[9], and Keizo Kinoshita[2]

[1]*Nagoya University, Nagoya 464-8601, Japan*
[2]*Osaka University, Suita, Osaka 565-0871, Japan*
[3]*The University of Tokyo, Bunkyo, Tokyo 113-8656, Japan*
[4]*University of California, Los Angeles (UCLA), CA 90095, U.S.A.*
[5]*University of Colorado, Boulder, CO 80309, U.S.A.*
[6]*Eindhoven University of Technology, 5600 MB Eindhoven, The Netherlands*
[7]*Pusan National University, Busan 609-735, Republic of Korea*
[8]*University of Antwerp, B-2610 Antwerpen-Wilrijk, Belgium*
[9]*Samsung Electronics Co., Ltd., Yongin, Gyeonggi 449-711, Republic of Korea*

*E-mail: ishikawa.kenji@nagoya-u.jp

Received March 10, 2017; accepted March 28, 2017; published online June 1, 2017

In this review, we discuss the progress of emerging dry processes for nanoscale fabrication. Experts in the fields of plasma processing have contributed to addressing the increasingly challenging demands in achieving atomic-level control of material selectivity and physicochemical reactions involving ion bombardment. The discussion encompasses major challenges shared across the plasma science and technology community. Focus is placed on advances in the development of fabrication technologies for emerging materials, especially metallic and intermetallic compounds and multiferroic, and two-dimensional (2D) materials, as well as state-of-the-art techniques used in nanoscale semiconductor manufacturing with a brief summary of future challenges.

1. Introduction

Transistor performance has been improved continuously through the further miniaturization of features. Currently, miniaturization is continuing through newly proposed nanoscale or atomic layer control processes. The development of new devices, such as transistors, memories, and emerging electrical circuit elements, is highly dependent on the establishment of these new dry processing techniques.

Historically, lithographic pattern-transfer technology and material etching processes evolved from wet to dry etching in the late 1970s. Dramatic increases in the etching rates of Si and Al through the use of halogen-containing gases for sputter etching were first described by Hosokawa et al.[1)] This technique was named reactive-ion etching (RIE), and has been widely used in microfabrication in the semiconductor industry. Parallel plate electrode plasma reactors [or capacitively coupled plasma (CCP) reactors] have been employed for RIE.[2–4)] Recognition of the importance of the ion energy and ion/neutral radical flux to the wafer surface allowed more highly controlled etching processes through the use of discharges driven by two or more power sources operated at the same or different frequencies. For example, charged particle and neutral radical densities can be controlled using high-frequency voltages, while ion acceleration across the sheath formed over a wafer surface can be controlled through the low-frequency voltage.[5)] RIE has been proven to be an indispensable technique in fabricating ultralarge-scale integrated circuits (ULSIs).[6,7)]

With the advent of Moore's law as the rule of thumb or as the business model of the exponential growth in semiconductor devices established in the 1960s, the semiconductor industry can continue integrating devices with increased functionality as long as processing solutions exist.[8)] Around 2005, the scaling-down scenario encountered various severe barriers and the approach of simple miniaturization was forced to diversify. Figure 1 shows a diagram of technology drivers, which is based on a figure in the report originally presented in the 2006 International Technology Roadmap for Semiconductors (ITRS).[9)] Continuation in the "*More Moore*" direction involves further miniaturization, ultimately reaching the "*Beyond Moore*" region, while the "*More than Moore*" direction explores a variety of emerging applications other than logic and memory devices such as analog, radio frequency (RF), passive, high-voltage (HV), high-power devices, sensors, actuators, and biochips. "*Heterogeneous integration*" is a combination of the two approaches and is employed in creating system on chip (SoC) and system in package (SiP) solutions.

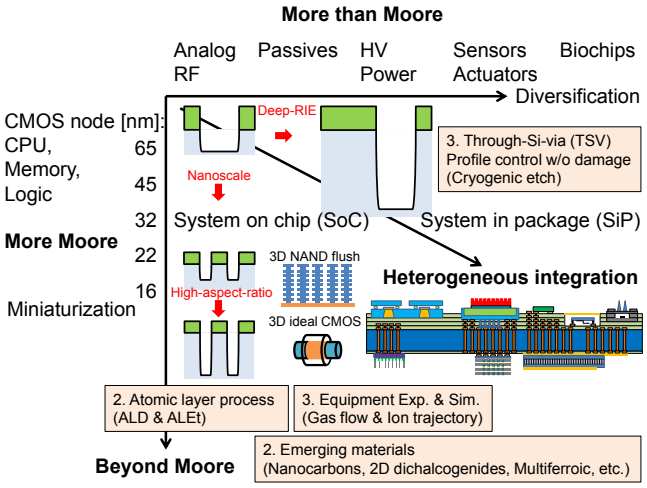

Fig. 1. (Color online) Technology drivers and a map of topics reviewed here. The diagram is based on a figure originally published in the 2006 ITRS with the addition of the reviewed topics.[9)] CMOS: complementary metal–oxide–semiconductor devices. CPU: central processing units.

In the *More Moore* approach, planar device structures are being replaced by nonplanar device designs such as three-

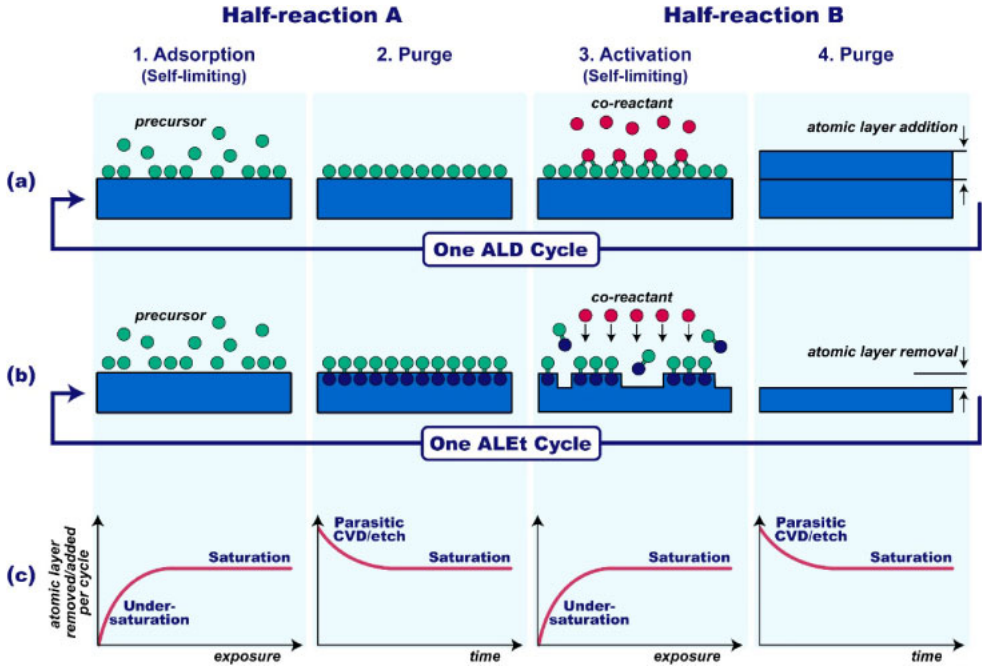

Fig. 2. (Color online) Schematic illustration of (a) ALD and (b) ALEt. In both cases, a generalized cycle is shown. (c) Saturation curves for the various steps in the ALD and ALEt processes.[13)]

dimensional (3D) gate stacks and vertical transistors. In 2008, Toshiba developed the 3D gate stack NAND flash memory, known as BiCS (3D stacked structure flash memory).[10)] Later, Samsung developed a stacked memory with more than 32 layers, called the V-NAND memory chip. Fabrication of the vertical gate stack structure requires high-aspect-ratio etching. In logic transistors, a similar transition from planar to 3D designs such as FinFETs can be observed, eventually leading to the development of a vertical transistor with a gate-all-around (GAA) structure. Fabrication technologies need to be revisited for such complex structures with various materials and nanoscale dimensions. To meet the challenges in the realization of patterning emerging device structures, plasma scientists and engineers must return to the first principles of RIE and ion-assisted reactions.

For the SiP approach, the etching technology for deep trenches as well as through-silicon vias (TSVs) needs to be developed alongside processes for patterning high-aspect-ratio features while both optimizing the feature profile and mitigating process-induced damage.

Furthermore, nanoscale electronics has been realized through the further development of fabrication technologies. Dry etching processes were first developed for insulators and dielectrics, followed by semiconductors. Beyond this trend, desirable etching technology needs to be developed for conductors. In *Beyond Moore*, multiferroicity, involving ferromagnetic, ferroelectric, and ferroelastic aspects, has received attention as a candidate technology driver. To date, only the physical sputtering process provides a means of patterning metal-containing materials. However, the physical sputtering process has disadvantages such as low etching rates, material damage,[11)] and redeposition.[12)] Anisotropic sidewall profiles can only be created by avoiding the redeposition of by-products with sufficient volatilities. Therefore, these emerging materials require a new technology for processing at the atomic level without damaging the materials.

Here we review nanoscale and atomic layer processing while focusing on two topics (1) advances in the development of atomic layer processing for emerging metal and intermetallic compounds, and multiferroic and two-dimensional (2D) materials, and (2) state-of-the-art fabrication technologies in semiconductor manufacturing for nanoscale control.

2. Advances in atomic layer processing for emerging materials

Atomic layer processes have become vital in the semiconductor industry, offering techniques capable of accurately controlling material properties and nanometer dimensions. These processes include atomic layer deposition (ALD) and now also atomic layer etching (ALEt). Both processes are shown schematically in Fig. 2.[13)] Most ALEt processes can be considered as a natural extension of the wide variety of conventional plasma-based etching processes.[14)] It is necessary to emphasize that atomic layer processes can be used for patterning with atomic-scale fidelity through self-limiting surface reactions while maintaining both the material properties and feature dimensions. In ALEt, the major requirement of material selectivity must be taken into consideration.

Renewed interest in the implementation of atomic-scale processing has emerged in the last three decades. In 1990, Horiike et al. reported their idea of separating each process for etchant adsorption and the removal of generated volatile products after chemical reactions. This process was named "digital etching".[15)] This approach was demonstrated by constructing a rotating disk apparatus equipped with a fluorine plasma source and an argon ion beam system.[16)] After that, they examined in detail the reaction of fluorine atoms and molecules on a Si(111) surface, and first reported the formation of a SiF monolayer, namely, they reported the realization of a self-limiting process for the Si/F system.[17)]

Self-limiting reactions are utilized in the thermal cyclic etching of SiO_2, i.e., the conventional etching of native oxides on an active silicon surface. A $(NH_4)_2SiF_6$-based modified layer forms on the surface of SiO_2 when it is exposed to etchants such as NH_3/NF_3-based or HF/NH_3-based chemistry.[18–33] These chemistries were commercialized in the semiconductor industry for use in precleaning technologies in film deposition, silicidation, and the fabrication of high-k dielectric metal gates.[29–33] Very recently, the thermal cyclic etching of SiN has also been realized.[34–36] In principle, a thin surface modified layer comprising $(NH_4)_2SiF_6$ forms on the surface in a self-limiting manner to protect a material from etching by preventing for the further exposure to etchants and can be removed by thermal annealing.[35]

Additional new processing techniques have been reported that involve chemically assisted ion beam etching (CAIBE) using Cl_2 plasma for etching GaAs. In 1992, Ludviksson et al. reported Cl_2 beam etching of GaAs,[37] whereas Meguro, Aoyagi, and coworkers reported self-limiting behavior in the ion beam etching of a chlorinated GaAs surface.[38–43] Matsuura and coworkers demonstrated the atomic layer-by-layer etching of silicon-related materials.[44–47] Many of these prior investigations were summarized by Kanarik et al. to show the compound effort and progress in atomic layer etching in the semiconductor industry.[14]

A very important merit of plasma processing is that it enables the deposition and etching of materials with high quality at low temperatures through the use of energetic species present within the discharge. From an industrial perspective, plasma-enhanced ALD at low temperatures has enabled self-aligned patterning, widely considered a breakthrough technology in the scaling of devices beyond the 20 nm node.[48,49] High conformality is a key feature in enabling this patterning approach. The low temperature ALD processes that have been reported include processes for oxides,[50,51] nitrides,[52–56] metals,[57,58] and other materials.[13,59–64]

In this section, we discuss how atomic layer reactions can be controlled in ALEt processing, especially in the case of emerging materials and processes. First, the works of George and coworkers on the ALEt of metal oxides and metal nitrides are reviewed. Control of the ligand-exchange during surface reactions is one critical point in this process. Surface fluorination plays a key role in ensuring effective ligand-exchange reactions for various metal oxides and metal nitrides. Second, studies by Chang and coworkers address the challenges in ALEt processes for metallic materials. The generation of stable substances having sufficiently high vapor pressures from the surface reactions is a necessary component in addressing the challenges in metal ALEt. Third, an overview of the work by Kessels et al. introduces the state-of-the-art in the area-selective ALD and atomic layer processing of 2D materials. Before our review of the above works, Table I lists a summary of reported ALEt technologies. We argue that discussions of the science and technology are more important than reviews of previous state-of-the-art techniques in ALEt.

2.1 Atomic layer etching of metal oxides and metal nitrides

The chemistry of thermal ALEt is based on fluorination and ligand-exchange reactions.[75,76] In the ligand-exchange reaction, a metal precursor accepts fluorine from a metal fluoride surface layer and concurrently transfers its ligand to the metal fluoride. This ligand-exchange can be characterized as a metal exchange transmetalation reaction between adjacent metal centers. Etching occurs if this reaction forms stable and volatile reaction products.

George and coworkers first reported thermal ALEt of Al_2O_3[75,76] and HfO_2[77] using HF as the fluorination reagent and $Sn(acac)_2$ as the metal precursor. Recent studies have demonstrated that trimethylaluminum [TMA, $Al(CH_3)_3$] can also be used as the metal precursor for Al_2O_3 ALEt.[78]

The use of TMA for Al_2O_3 ALEt is of special interest because this metalorganic compound is typically used for the ALD of Al_2O_3. HF and TMA can etch Al_2O_3 at rates of 0.14–0.75 Å/cycle at 250–325 °C, respectively.[78] The temperature dependence of the Al_2O_3 etching rate is correlated with TMA removing a greater fraction of the metal fluoride layer at higher temperatures, where a quartz crystal microbalance (QCM) was used to measure the results for 100 cycles of Al_2O_3 ALEt using HF and TMA.[78]

The ligand-exchange reactions during thermal ALEt provide pathways for selective ALEt, while plasmas can be used together with thermal ALEt to enhance surface reactions by exploiting energetic charged and neutral species within the discharge.[75,79] The gas-phase nature of the reactants in thermal ALEt also facilitates conformal ALEt in shadowed high-aspect-ratio structures.

In selective ALEt, one material is etched preferentially in favor of other materials. Selective ALEt can be achieved via the ligand-exchange process.[79] When it accepts fluorine from the metal fluoride layer, the metal precursor donates a ligand to the metal in the metal fluoride and forms a reaction product. Depending on the nature of the ligand, the reaction products formed after ligand-exchange have distinct stabilities and volatilities. Differences in the stability and volatility of the reaction products can be used to achieve selective ALEt. George and Lee observed different rates for ALEt using sequential HF and TMA exposure on TiN, SiO_2, Si_3N_4, Al_2O_3, HfO_2, and ZrO_2 thin films at 300 °C.[79] These films were all etched together under identical conditions. Sequential HF and TMA exposure can be used to etch Al_2O_3 and HfO_2. The etching rates during Al_2O_3 and HfO_2 ALEt were 0.45 and 0.10 Å/cycle, respectively. No etching was observed for sequential HF and TMA exposure on TiN, SiO_2, Si_xN_y, or ZrO_2. This selectivity can be understood in terms of the stability and volatility of the reaction products.

Thermal ALEt can also be applied for the ALEt of metal nitrides using HF and $Sn(acac)_2$. AlN ALEt was measured as a function of the number of ALEt reaction cycles at 275 °C using in situ spectroscopic ellipsometry (SE).[80] A low etching rate of ~0.07 Å/cycle was measured during the etching of the first 40 Å of the film. It was postulated that this small etching rate corresponded to the etching of the AlO_xN_y layer formed on the AlN film. The etching rate then increased to ~0.36 Å/cycle for the pure AlN film.

Adding a H_2 plasma step following each $Sn(acac)_2$ exposure increased the AlN etching rate from 0.36 to 1.96 Å/cycle. This enhanced etching rate is believed to result from the ability of the H_2 plasma to facilitate the removal of acac species from the surface that may limit the AlN etching

Table I. Summary of reported atomic layer etching of materials with their corresponding adsorbed surface modification chemistries and etching energy sources. Each material is classified into a subset of semiconductor or oxide.

Material	Modification chemistry	Energy source	E_{ion} (eV)	Etching rate (Å/cycles)	Selectivity	Anisotropy	Ref.
Semiconductor							
AlN	$Sn(acac)_2$/HF	Thermal	—	0.36–1.96	—	No	80
GaAs	Cl_2	Ar^+	22	~14	—	—	38, 39, 41
	Cl/Cl_2		20	~3	—	—	40, 65
Ge	Cl_2	Ar^+	~13	1.5	—	—	45, 46
Si	CF_4/O_2,	Ar^+	~20	3.0	—	Yes	15, 16
	NF_3/N_2, F_2/He plasmas		10	0.5–2.5	—	—	44, 45
	Cl_2		20	1 ML/cycles	—	—	66
	Cl_2/Ar plasma		40	~15	∞ to SiO_2	Yes	14, 67, 68
MoS_2	Cl	Ar^+	<20	1 ML/cycles	—	—	69
	O_2 plasma	Thermal	—	1 ML/cycles	Possible	—	70
Graphene	O	Ar	~30	1 ML/cycles	—	—	71
Oxide							
Al_2O_3	$Sn(acac)_2$, HF	Thermal	—	0.14–0.61	—	No	75
	$Al(CH_3)_3$, HF	Thermal	—	0.14–0.75	Possible	No	79
HfO_2	$Sn(acac)_2$, HF	Thermal	—	0.07–0.12	—	No	77
ZnO	$Al(CH_3)_3$, HF	Thermal					81
SiO_2	CHF_3	Ar plasma	20–30	~1–4	—	—	72, 73
	C_4F_8		<30	~4	to Si	—	
	$Al(CH_3)_3$, HF	Thermal			—	No	82
$^*Si_3N_4$	H_2 plasma	Ar^+/H_2	100 (H^+)	~20–60	—	—	47
						—	74
	CHF_3, C_4F_8	Ar plasma	20–35	4–12	to SiO_2		72

rate. Adding Ar plasma exposure after each $Sn(acac)_2$ exposure also increased the AlN etching rate from 0.36 to 0.66 Å/cycle.

The conformality of ALEt is also necessary to evaluate the self-limiting reactions. The self-limiting nature of the fluorination and ligand-exchange reactions, which define thermal ALEt, leads to isotropic etching. If gas exposure times are sufficiently long to allow the surface reactions to reach completion, thermal ALEt has the potential to etch conformally, complementing the ability of ALD of conformal deposition in high-aspect-ratio structures. The conformality of ALEt has been demonstrated in trench structures defined using thin metal foils clamped between silicon substrates.[79] The ALEt of Al_2O_3 films in a trench with an aspect ratio of 64 (30 mm long and 3 mm wide) was realized. The height of the trench was defined using a 0.254-mm-thick steel foil. The initial Al_2O_3 film was deposited by Al_2O_3 ALD. The Al_2O_3 film was etched by 200 cycles with HF and TMA at 300 °C using reactant pressures of 0.15 Torr.

George and Lee pointed out that ALEt can be accomplished using sequential, self-limiting fluorination and ligand-exchange thermal reactions.[79] This thermal ALEt has been demonstrated for various metal oxides and metal nitrides such as Al_2O_3 and AlN (Table I). The thermal reactions provide pathways for selective ALEt. In addition, plasmas can be used to enhance thermal ALEt. The gas-phase reactants for thermal ALEt also allow conformal ALEt in high-aspect-ratio geometries.

2.2 Atomic layer processing of multiferroic materials

Multiferroic materials, exhibiting ferroelectricity and ferromagnetism simultaneously, have attracted interest for energy-efficient nanoscale multifunctional applications.[83] Owing to the scarcity of single-phase multiferroics in nature and their weak responses at room temperature, engineered composites have been explored to realize robust multiferroic behaviors by coupling the functional properties from the constituent phases. A strain-mediated coupling strategy relies on interfacing magnetostrictive and piezoelectric materials. However, such a strain-mediated approach in thin-film composites is limited by the interfacial area and interfacial contact quality. ALD is thus an ideal technique for synthesizing multiferroics composite.[83]

For the synthesis of multiferroic composites, ALD processes for $BiFeO_3$ (BFO) and $CoFe_2O_4$ (CFO) thin films were realized on $SrTiO_3$(001) substrates with tmhd-based (tmhd = 2,2,6,6-tetramethylheptane-3,5-dione) metalorganic precursors and atomic oxygen. The use of atomic oxygen as the oxidant enables low-temperature processing. The BFO films showed epitaxial single-crystalline growth in the (001) pseudo cubic orientation after thermal annealing [Fig. 3(a)], while the CFO films were polycrystalline due to the lattice mismatch between the film and substrate.[84] The ferroelectric and magnetic properties were respectively confirmed using piezo-response force microscopy (PFM) and superconducting quantum interference device (SQUID) magnetometry [Figs. 3(b) and 3(c)]. Tunable CFO magnetic proper-

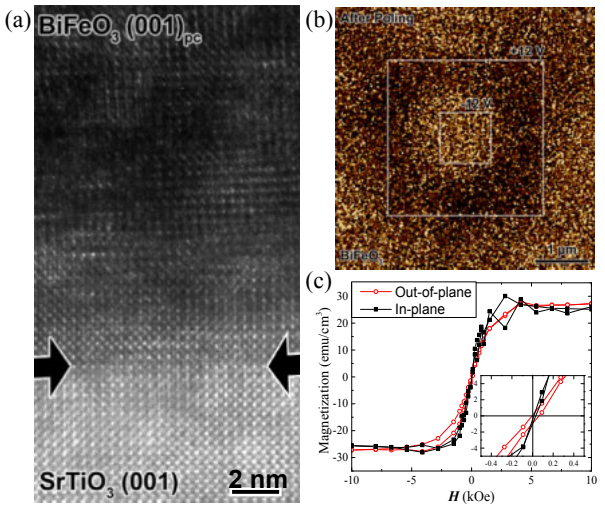

Fig. 3. (Color online) (a) Cross-sectional TEM image of $BiFeO_3$ thin film deposited on $SrTiO_3$(001) substrate via RE-ALD, showing single crystalline epitaxial growth. The film was annealed at 650 °C for 1 min in O_2. Arrows indicate the interface. (b) PFM phase image of the $BiFeO_3$ film. The phase contrast between different poling regions indicates the ferroelectric nature. (c) Room temperature magnetic hysteresis loops of the $BiFeO_3$ film, showing a weak ferromagnetic response due to antiferromagnetic spin canting.[84]

ties were demonstrated by thickness-related strain relaxation measurements.[85]

Chang and coworkers have pointed out that multiferroic materials are capable of enabling energy-efficient designs for many devices, including memory, antennas, and motors. ALD and ALEt are processes enabling the integration of these materials.[86,87]

2.3 Towards the ALEt of metals

One important building block for realizing multiferroic composites is the ferromagnetic material, such as Co, Fe, or CoFe, as well as doped alloys such as CoFeB. Noble metals with large spin–orbital coupling such as Pt and Pd are also important for spin-based nanoelectronics. Due to the etch-resistant nature of these metals, noble ion beam milling is widely used for patterning.[88,89] Additional methods include methanol plasma etching, which requires further improvement in maintaining the etching selectivity and pattern transfer fidelity for high aspect ratio features.[88–91] ALEt can be partly considered as the reverse of ALD, and through the utilization of chemistries inspired by ALD precursors, can be controlled by exploiting the self-limiting nature of one of the surface reactions. Table II summarizes the general characteristics of ALD and ALEt, including the advantages of using thermal and plasma-enhanced ALD/ALEt, namely, the ability to achieve anisotropy using charged species as well as precise composition control and selectivity.

Kim et al. have developed an approach to the plasma etching of magnetic materials that uses a combination of thermodynamic assessment and experimental validation.[92] Potential reactions between the dominant vapor phase and condensed species at the surface were considered under various process conditions. The volatility of the etching products was calculated to aid the selection of patterning chemistries, and this approach has been demonstrated successfully for test cases involving both halogen and organic etching chemistries.[93,94]

Table II. Summary of key characteristics of atomic layer deposition and etching.

ALD	ALEt
At least one self-limiting reaction	At least one self-limiting reaction
Gas-phase processing, surface reaction	Gas-phase processing, surface reaction
Thermal → conformality	Thermal → isotropy
Plasma enhancement → High quality at low temperatures, potentially reduced conformality	With ion bombardment → anisotropy
Very thin film with **precise composition**	Very thin film with **selectivity**
Widely used for oxides	Demonstrated for oxides
Demonstrated for semiconductors	Limited demonstration for semiconductors
Limited demonstration for metals	No demonstration for metals

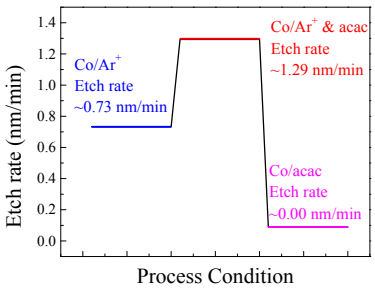

Fig. 4. (Color online) Synergy plot showing etching rate of Co by Ar^+ ions only (0.7 nm/min), Co in acac vapor only (negligible), and enhanced etching rate by alternating exposure of Ar ion beam and acac vapor to etch Co (1.3 nm/min).[94]

One major consideration for enabling the ALEt of metallic and intermetallic thin films is the transformation of the metallic surface through physical or chemical means. Work on the use of Ar^+ in conjunction with acac chemistry has shown that ionic bombardment of cobalt thin films results in physical modification of the surface, generating additional active surface sites, disrupting the Co lattice by Ar bombardment, and allowing acac ligands to bond with Co to form $Co(acac)_2$, using a cycle etching process. The increased etching rate from this cyclic process, compared with that from pure physical sputtering and only chemical exposure, demonstrates the synergy between Ar^+ irradiation and acac vapor exposure. Impinging ions facilitate both the binding of acac ligands through the generation of surface sites and the removal of $Co(acac)_2$ in subsequent ion beam exposure (Fig. 4). These observations verified thermodynamic calculations performed for the Co-acac system and confirmed the efficacy of volatile organic chemistries used in conjunction with physical or chemical modification for etching metallic thin films.

An additional approach has shown that exposure to O_2 plasma to convert a metal to a metal oxide is the most effective approach for chemically modifying transition (Fe, Co, Cu) and noble (Pd, Pt) metal surfaces and enabling the selective removal of the metal oxide using both solution and vapor-phase etching processes.[95] A highly etching selectivity of the metal oxide relative to the metal by organic vapor was achieved, suggesting that one of the most important requirements in atomic layer etching, a self-limiting reaction, was

satisfied.[96] By tuning the oxide thickness generated by O_2 plasma exposure, the etching of metals can be controlled at an atomic level.[95–98]

2.4 Next steps in atomic layer processing

Area-selective deposition is another approach garnering much attention.[49] In ALD, the precursor adsorption process depends strongly on the surface chemistry, and therefore can be limited to a part of the substrate through local modification of the surface properties. For example, area-selective ALD can be obtained when precursors selectively adsorb on areas whose surface is OH-terminated. One common approach utilizes partial surface deactivation so that ALD does not take place in these regions, for example, by using self-assembled monolayers (SAMs). Alternatively, a surface can also be activated locally so that growth only takes place in these regions. The main challenge for such area-selective ALD processes is area activation as well as the suppression of nucleation on the non-activated surface.[45]

The processing of 2D materials such as graphene and 2D transition-metal dichalcogenides such as MoS_2, $MoSe_2$, and WSe_2 is another hot topic, which was recently reviewed by Jesse et al.[99] One processing route employs focused ion beams (FIBs). The FIB-induced deposition and etching of nanoscale materials has historically been dominated by the use of a liquid metallic gallium ion source.[100] While a practical beam resolution of up to 10 nm has made it the preferred technique for direct-write deposition and etching,[101] gallium staining in the near-surface region of the substrate/growing material limits its use in many applications. The push for finer material control has led to the development of higher-resolution ion sources such as the gas field ion source microscope, and He^+/Ne^+ gas field ion source microscopes have recently been commercialized.[102] The He^+ source has sub-1-nm resolution,[103] whereas the Ne^+ source has a theoretical resolution of 1 nm.[104] This area of study is rapidly growing and can achieve the atomic-scale manipulation of materials to fabricate subnanometer-scale features. See, for example, Ref. 105.

Kessels et al. have also pointed out that plasma-based processes will be indispensable for preparing and patterning 2D transition-metal dichalcogenides, which are considered key materials in next-generation device manufacturing.[13] When these materials consist of no more than a few monolayers, control at the atomic-layer scale is of utmost importance to meet the extremely stringent requirements imposed by nanoscale devices. Further progress in atomic layer processing methods such as ALEt and (area-selective) ALD is therefore vital.

3. State-of-the-art in semiconductor manufacturing for nanoscale control

As described in the introduction using Fig. 1, the technology drivers for semiconductor memory devices have transitioned from the scaling down of 2D patterns to the use of 3D vertical stacks of memory elements, such as BiCS and V-NAND. Such the breakthrough beyond no pattern limitation solved the issue. Meanwhile, more challenges offer advances in the technology integration especially for the plasma etching process of high-aspect-ratio contact holes (HARC) etching. In addition, SiP technology depends on deep reactive ion etching (DRIE), enabling high-aspect-ratio features. HARC

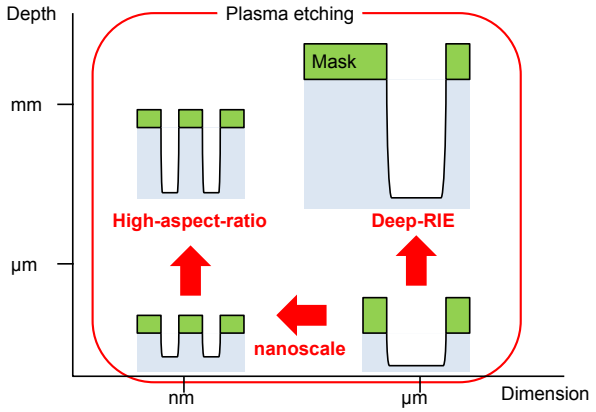

Fig. 5. (Color online) Technology roadmap of plasma etching. (1) Nanoscale and atomic layer etching (smaller feature dimensions) and (2) DRIE at micron scale (increased depth of features). Another challenge is HARC etching with no pattern limitation.

etching and DRIE are currently used to create high-aspect-ratio features with dimensional scales on the order of nanometers and microns, respectively, as shown in Fig. 5. The fabrication of these anisotropic features with high aspect ratios is essential to meet the requirements for reactions on material surfaces to maximize anisotropic etching properties without any material damage.

Conventionally, the radical-to-ion ratio has been the most important factor in such considerations. To achieve the etching of large-size wafers with high production yields, plasma etching processes have been required to control the trajectories of ions impinging on the surface through acceleration across the sheath from bulk plasmas. Meanwhile, the concentrations of both reactants and by-products in the gas phase depend locally on the wafer position and temperature. In dry etching processes, it is very important to control the variation of at least three parameters, with the most important being the ion energy/trajectory, radical composition/concentration, and wafer temperature. Here we discuss the plasma etching process at the nanoscale from the perspective of plasma physics and plasma–surface interactions. Emphasis is placed on three key topics: ion trajectories, the concentration of radicals, reactants, and side products, and the wafer temperature.

3.1 Ion trajectories in high-aspect ratio etching

Further patterning technology must be addressed in the development of high-aspect-ratio features. Well-tuned control of the process uniformity across the wafer during plasma etching processes is often a serious issue in mass production since controlling the process variability to achieve repeatable results is always important for meeting yield and device performance requirements. The ratio of ions to neutrals is a key parameter in reducing variability. Since the introducing of single-wafer processing in the early 1980s, etching chambers have been designed to produce similar plasma conditions on the entire wafer to achieve uniform processing results.[106] Electrical and chemical discontinuities at the edge affect the uniformity across the wafer. Voltage gradients can also be created at the wafer edge due to the change from a biased surface to a grounded or floating surface, which results in further variation. These gradients bend the plasma sheath at the wafer edge, changing the trajectory of ions relative to the wafer.[106]

Babaeva and Kushner have reported on the effects of the height and electric properties of a focus ring, which was placed around a wafer.[107] The energy and angular distribution functions of ions penetrating into the narrow gap between the wafer and the adjacent focus ring were simulated.[107] Maeda et al. reported simulation results for the incident angle of ions at a wafer edge, assuming the trajectories of collisionless ions with background neutrals.[108] Experimental results have also been shown for conditions under which the bias potential on a focus ring was controlled.[108] Similarly, Kubota et al. estimated the angle of the etched profile near large structures from ion trajectories.[109] Denpoh reported the distortion of ion trajectories near a wafer edge.[110]

Um et al. pointed out that the focus ring plays a very important role in leveling the sheath profile at a wafer edge and maintaining the uniformity of the plasma despite the presence of electrical discontinuity at the wafer edge. The incident ion trajectory is governed by the sheath, which was determined by coupling plasmas with the focus ring structure, and they investigated the power transfer efficiency as a function of the applied bias voltage. This phenomenon for ion trajectory was calculated successfully by plasma simulation, and a suitable design of the focus ring was suggested for achieving an uniform incident ion angle at a wafer edge. On the basis of this model, a new method for the dynamic control of a sheath on a wafer edge has been introduced.[111]

3.2 Effects of temperature on surface reactions for damage-free etching

Cryogenic etching was first proposed in 1988.[112–114] Originally, etching at temperatures below 0 °C was expected to resolve issues in the silicon etching processes by mitigating the spontaneous etching of undesired regions by fluorine in order to improve material selectivity and feature profiles. During plasma processing, since reactive ions assist etching, wafer cooling is utilized to reduce unwanted reactions such as spontaneous etching and those causing material damage. Bestwick et al. reported the selective removal of sulfur fluoride (SF_x) species on a cooled electrode and showed that the resulting plasma was dominated by F and F_2 species.[115] In 1990, Mizutani et al. reported plasma-induced damage on SiO_2 and that the damage to the Si interface was reduced effectively when plasma processing was performed at low temperatures.[116] The mechanism was reported to be the suppression of the hole-trapping nature following the VUV generation of electron–hole pairs.[116] Varhue et al. reported that the spontaneous sidewall etching reactions of organic polymer photoresists were also inhibited at cryogenic temperatures.[117] Hara et al. reported that the fluorine gas generated during fluorine-based dry etching diffuses into low-*k* films, especially porous low-*k* films. This problem was solved by low-temperature (−25 °C) etching.[118]

Recently, the high-aspect-ratio silicon features with high mask selectivity and smooth sidewalls have attracted much attention for the mass production of ULSIs and micro-electromechanical systems (MEMS). For example, the DRIE technologies were introduced in the review of Wu et al.[119] The Bosch process is conducted by cyclic treatments comprising the passivation of feature sidewalls by C_4F_8 plasma and the etching of feature bottoms by SF_6 plasma or XeF_2 gas.[119] Also, reactive etching by ClF_3-Ar neutral cluster beam etching was reported.[120,121] The actual fabrication of high-aspect-ratio Si structures by this method was reported.[122–125] Chemical dry etching technologies based on fluorine etching reactions in NO and F_2 mixtures were found to be highly dependent on the wafer temperature.[126,127] Therefore, the wafer temperature was identified as an important factor in controlling surface reactions during plasma processing.

The cryogenic etching of silicon has been investigated by Dussert and coworkers,[128,129] and Ishchuk et al.[130] However, a fundamental understanding of the cryogenic etching process with plasmas containing SF_6/O_2 and C_4F_8 has not yet been obtained. Specifically, the plasma behavior and its interaction with the surface to improve cryogenic etching need to be investigated. Tinck and coworkers applied numerical models and performed experiments to clarify the plasma behavior and plasma–surface interactions.[131–134] The effects of the wafer temperature, ranging from 173 to 293 K, and gas flow rates on the plasma and on the etching process need to be discussed to elucidate differences in the surface reaction mechanisms during etching. The importance of layers of physisorbed species formed at cryogenic temperatures was identified on the basis of these experimental and computational results, along with the effect of the wafer temperature and the influence of the oxygen gas feed fraction.

3.3 Simulations of plasma dynamics and chemical reactions in plasma reactors

The importance of simulation-based research is rapidly increasing as the feature size decreases while the chamber size increases. It is difficult to include every parameter involved in realistic industrial applications in plasma simulations. Capacitively coupled plasmas (CCPs) are widely used in dry processes for etching and deposition in semiconductor manufacturing. A particle-in-cell (PIC) simulation[135] is suitable for nonlinear, transient, and nonlocal kinetics, but this approach encounters difficulties in calculations at larger scales and higher gas pressures. Another approach is to calculate the bulk plasma with a model based on fluid mechanics.[136] It is difficult to accurately include chemical reactions because of imperfect reaction data, especially for heavy-particle interactions. The plasma surface interaction is needed to consider reactions occurring at the atomic scale; therefore molecular dynamics (MD) calculations are powerful tools for understanding reaction occurring at the etched surfaces.[137,138] However, the mechanism is frequently unknown and there is little surface reaction data for targeted etching reactions. Numerous feature scale simulations have been presented.[139,140] Kuboi et al. recently reviewed advances in simulation technology for etching processes.[141]

A numerical 2D fluid simulation of CCP has been presented for a plasma enhanced chemical vapor deposition (PECVD) reactor,[142–144] and a hybrid plasma equipment model (HPEM) was developed by Zhang and Kushner.[145] The hybrid model treated collisions using a Monte Carlo collision (MCC) approach,[142] combined with the chemical reactions of neutral species in a fluid model.[143,144] Kim and Lee analyzed the effects of electrode spacing and a 3D gas flow from a shower head for a $SiH_4/NH_3/H_2$/He discharge.[143,144]

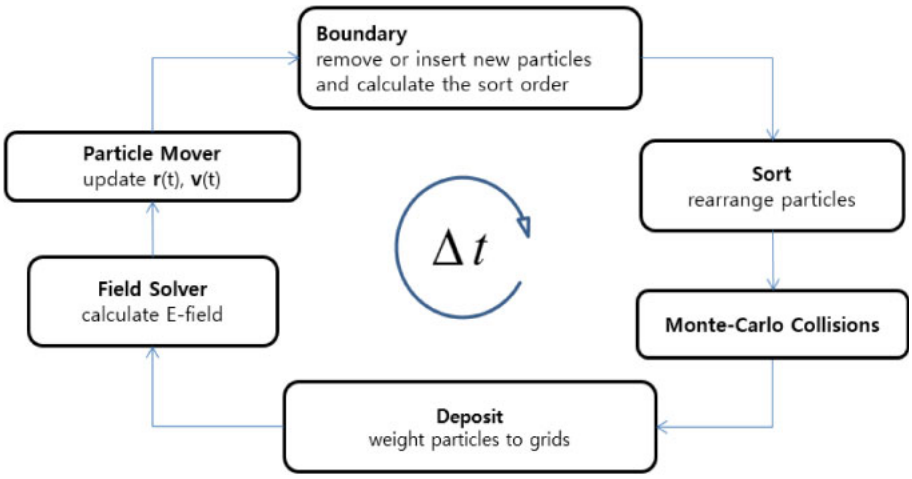

Fig. 6. (Color online) Flow chart of a GPU-PIC model with a cell-based memory arrangement.

For PECVD discharges, PIC simulations are computationally expensive because of the relatively high gas pressure of Torr order and high plasma density. Recently, Lee et al. demonstrated an approach to PIC simulation for CCP deposition with the advantage of decreased computational time through parallelization using graphic processing units (GPUs). In order to increase the simulation speed of a PIC code, a cell-based memory arrangement for the storage of superparticles is adopted. Figure 6 shows a flow chart of the GPU-PIC simulation, which requires a sort subroutine in order to rearrange the particle sequence for each cell to enhance the simulation speed. This data structure was combined with the CUDA library in order to use GPUs effectively. With the help of parallelization, the final speed of the parallelized GPU-PIC code is up to 100 times that of a serial code with a single CPU, which makes it possible to run a 2D PIC simulation of CCP in a deposition reactor at a pressure of Torr order. Lee et al. pointed out that the transient and kinetic effects should be considered in plasma reactions as a function of the electron energy distribution, and importantly, that the gas flow velocity profiles affect the deposition rates determined by the precise calculation of the distribution of reactive species.

Figure 7 shows the results of 2D CCP simulation at a Torr-order gas pressure. The driving electrode at the top is driven with an RF power at 13.56 MHz, and the ground electrode is located inside of the dielectrics at the bottom under the substrate. The left wall has a symmetric boundary condition and the right wall is grounded. The dielectrics have a relative permittivity of 9 and the total power is fixed to 350 W. The grid size is 0.02 cm in each direction and a time step of 1.44 ps was used to treat the MCC accurately. It was observed in the simulation that the number density of excited states increases rapidly as the gas pressure increases. In each case in Fig. 7, the density of metastable excited states is approximately 10 times larger than that of electrons. In this case, the effect of step ionizations is more important than the direct ionization for electron impact collisions because the ionization threshold energy is much lower for step ionization than direct ionization. In addition, heavy-particle interactions are also important. However, here is insufficient reaction data for heavy-particle reactions.

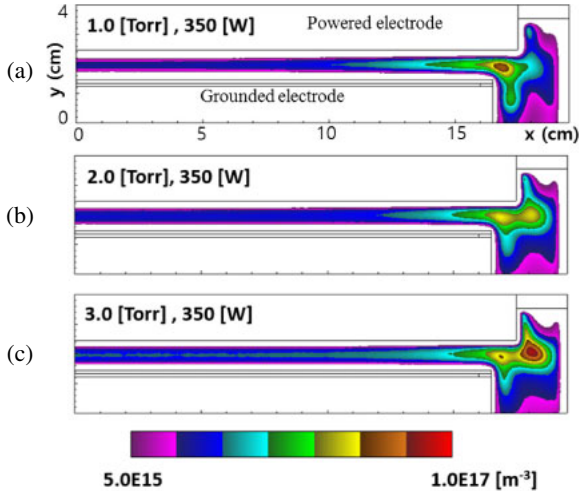

Fig. 7. (Color online) Time-averaged electron density profiles of a CCP discharge with a pure Ar gas using the GPU-PIC simulation code for pressures of (a) 1 Torr, (b) 2 Torr, and (c) 3 Torr with a fixed power of 350 W and a driving frequency of 13.56 MHz.

4. Future challenges

To consider the question, "How we can control the surface reactions at the atomic scale?", we must define the surface during dry processing. Actual surfaces etching reactions differ from well-defined surfaces in surface science. Although the two surfaces are considerably different, an atomic-scale understanding of ALEt still requires detailed technological and scientific examination of the plasma–surface interactions.

Well-defined surfaces have the favorable characteristic of chemically activated sites owing to the presence of dangling bonds. On the other hand, a number of dangling bonds on an actual surface are terminated. In both cases, the surface catalyzes a variety of chemical reactions. Often, surface reactions take place with kinetic control regardless of thermal equilibrium. Namely, nonequilibrium should be considered and modeled in this field.

During plasma processes, complexity also arises from the involvement of a myriad of species such as electrons, ions, radicals, and photons generated in the plasmas. These plasma components also contribute to the nonequilibrium dynamics

of the surface reactions. Namely, a dynamic equilibrium should be preferentially considered. Actual surface reactions can then be analyzed with real-time in situ diagnostics.

By understanding surface reactions, measurement and analysis of the plasma parameters and chemistry allow their correlation to changes in the surface, thus enabling further tuning of each process. Focusing on the plasma components, generation and transport in the reaction chamber should also be considered. The pressure determines the frequency of collisions with other molecules in the gas phase and also the frequency of collisions with the walls, resulting in collisional transport at high pressures and collisionless transport at low pressures. The motions of electrically charged particles in plasmas thus determines the sheath formation over the surface, which can be represented on the basis of electromagnetism.[3,4] The sheath forms a negative potential on the wall surface. As a result, ionic species are accelerated across the voltage potential and impinge upon the substrate surface. In addition, neutral species undergo transport via diffusion or kinetic motion with only thermal energy. A fully developed model of the transport of species in processing situations still remains a challenge.

Ionic and neutral species interact with the surface material, resulting in adsorption and the subsequent desorption of sufficiently volatile products. The surface processes in adsorption occur under both thermodynamic and kinetic control.[146] The desorption process depends on the temperature of the surface. Notably, the dynamic equilibrium of the surface reactions should be analyzed. Causal relationships may then appear for subsequent reactions. For example, in ion beam experiments, the experimental etching rates are sometimes represented by a nonlinear relationship with the ion dose, since the ion-irradiated surface modification affects the determination of etching yields.[147–150]

When considering the dynamic equilibrium, the wafer temperature is indeed an important parameter for determining reactions. Wafer temperatures play a key role during the plasma processes, when the process seemed to be nonequilibrium. Donnelly and McCaulley reported an optical interferometric technique for measuring silicon wafers.[151,152] Recently, Koshimizu et al. and Tsutsumi et al. reported the results of rapid (ms) real-time temperature monitoring in plasma etching processes.[153–155] The temperature variations across a wafer and a focus ring were found to evolve owing to differences in heat transport involving the heat capacity and thermal contact resistances.[154] Although the temperature control of chamber parts tends to be lacking in consideration, experiments and simulations are needed to reveal the dynamic equilibrium in real time. There is a need for the comprehensive understanding of dynamic equilibrium.

As mentioned above, the complexity of atomic-scale surface reactions prevents them from being well controlled. The surface reactions during dry etching are simply represented by $R(gas) + S \rightarrow R\text{–}S(surf) \rightarrow RS(gas)$, where R stands for gaseous reactants, and S is a material atom on the surface. The R–S bonding on the surface is described via the processes of physisorption and chemisorption. The adsorption and absorption phase (the first arrow) is broadly considered to be complex formation of the inorganic materials with coordination chemistry. Figure 8 schematically shows a dissociation path in the coordination reaction

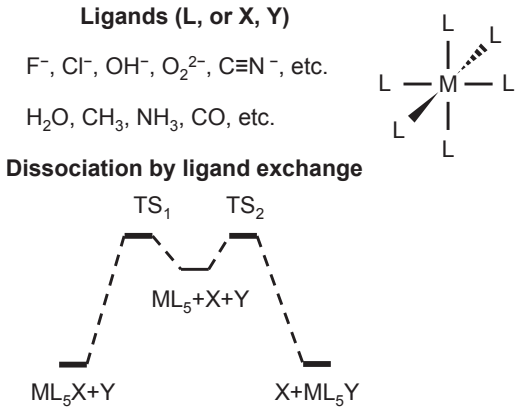

Fig. 8. Dissociation by ligand exchange. M is the central metal, and TS_1 and TS_2 are the transition states.

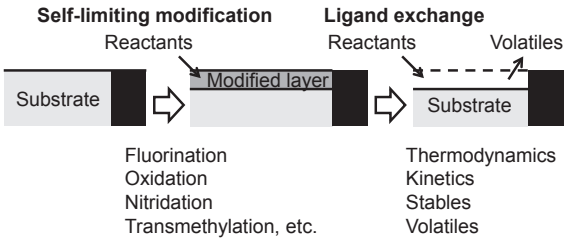

Fig. 9. Schematic diagram showing the principle of thermal atomic layer processing based on ligand exchange reproduced from George et al.[79]

for a complex involving a central metal atom (M) coordinated with ligands (L). Subscripts represent coordination numbers and this octahedral structure usually has six ligands. The targeted ligands are represented by X and Y. An arbitrary intermediate state and transition states are also represented. If the first step is self-limiting and material-selective, then a volatile reaction product resulting from the ligand-exchange enables atomic-level processing. This representation is valid for reactions in conventional dry processes. In dry etching, these volatile products are frequently formed by the coordination of ligands such as halogens.

Figure 9 shows George's scheme for atomic layer processing via coordination and ligand-exchange reactions. Under this scheme, the modified layer is self-limiting and exhibits material selectivity. In ALEt, the selective modified layer plays an important role in determining the ALEt properties.

Challenges remain in ALEt of metallic surfaces. To date, particularly in the 1990's, copper etching has been mainly studied.[156] Levitin and Hess summarized the difficulty of etching copper using a chemical vapor via copper oxidation.[157] On the metallic surface, electrons are delocalized. First oxidation or chlorination of the copper surface was performed to ensure the self-limiting modification. The introduction of a secondary H_2 plasma removed the CuCl layer. β-diketones such as 1,1,1,5,5,5-hexafluoro-2,4-pentadione, H^+(hfac),[158–161] organic acids,[162–166] and other chemistries[167–180] have been shown to react with and remove copper oxides. However, copper oxides with different oxidation states, such as cuprous oxide Cu^I_2O and cupric oxide $Cu^{II}O$, were shown to react differently with H^+(hfac): $Cu^{II}O + H^+(hfac) \rightarrow Cu(hfac)_2\uparrow + H_2O$ and $Cu^I_2O + 2H^+(hfac) \rightarrow Cu^0 + Cu(hfac)_2\uparrow + H_2O$. No reaction was

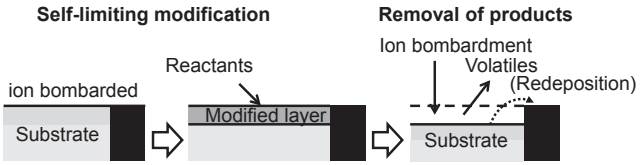

Fig. 10. Schematic diagram detailing implementation of directional ALEt through the use of ion bombardment utilizing a two-step process comprising of (1) a modification step generated by ionic bombardment with a subsequent reaction and (2) a removal step wherein impinging ions facilitate the selective removal of etching products to regenerate the original surface.

observed for Cu^0 and H^+(hfac). Therefore, if Cu^I is present on the surface, both Cu^0 and Cu^{II} are generated as a result of the reaction of H^+(hfac). Cu^{II} is removed by volatilization but Cu^0 is not, eventually resulting in a buildup of Cu^0 and termination of the copper removal process.[157] Thus, for metal ALEt, it is necessary to explore how to create local reaction sites with nonmetallic character, namely, those free from conjugated electrons and volatilization of the reaction products.

One approach utilizes a gas-cluster beam under acetic acid vapor to etch Pt, Ru, Ta, CoFe, and other materials.[181–185] Another approach utilizes noble ion bombardment in a preadsorption step with subsequent exposure to reactants, followed by a removal step with volatile products, as shown in Fig. 10. The resulting modified layer consists of a physically changed material that is chemically identical to the underlying substrate but has a different density and weaker bonding due to disruptions in the lattice, as well as an increased number of active surface sites to which reactants can bond and form volatile products. Kanarik et al. argued that ion bombardment provides energy to break the bonds underneath the modified layer.[14] The advantage of using ions is that they can be accelerated toward the wafer to provide the benefit of directionality.[186] A high ion energy is required due to the inefficiency in transferring the ion energy to the target bond. Energy is deposited by the impinging ion entering the subsurface region, leading to a collision cascade in the substrate material.[14,186] A similar approach has been demonstrated using noble ion beam irradiation to physically modify preadsorption metal surfaces and remove volatile etching products with subsequent ion exposure.[94] In an effort to enable higher etching rates and achieve additional selectivity for the dry etching of metallic thin films, reactive oxygen plasmas have also been shown to be effective for the directional chemical modification of transition and noble metals through the generation of a thin metal oxide surface layer upon the application of a bias voltage to the substrate. Chen et al. demonstrated the chemical contrast produced using reactive ion bombardment with the subsequent delivery of vapor-phase organics to the modified surface, resulting in an anisotropic and self-limiting etching process capable of achieving greater selectivity to the underlying metal.[96]

A dilemma occurs in self-limiting modifications, and a problem is that stable by-products at room temperature tend to be nonvolatile and vice versa. In brief, the volatilities of the etching by-products are determined by the chemical nature of the bonding when forming the solid phase, which in turn depends on molecular weights, intermolecular forces, and so forth. Also, chemical bonds are the origin of the

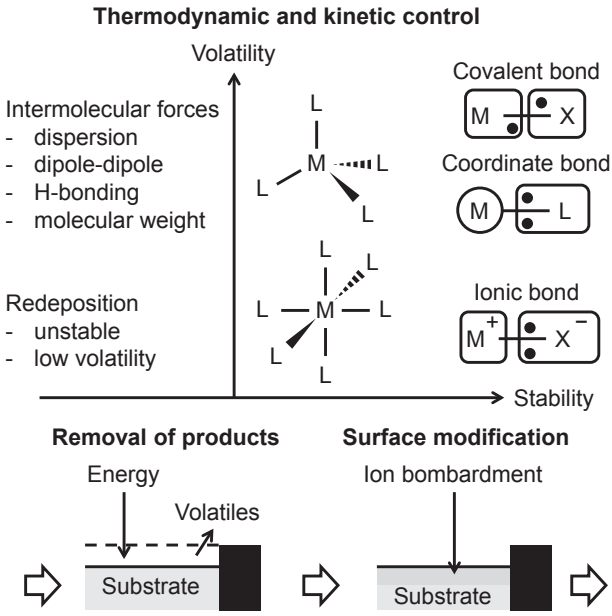

Fig. 11. Atomic chemical engineering in product formation in ALEt. The volatility and stability of the products may correlate with each other. This is briefly explained in the main text in terms of intermolecular forces and chemical bonds.

stability of products (Fig. 11). Similarly to the complex formation of metal-ligand systems, electron donation plays an important role in resolving this dilemma.

In plasma processes, the reactive species in the surface reactions can be utilized, i.e., kinetic control schemes. For instance, atomic species react and etch spontaneously in the case of etching bare aluminum with chlorine and also tungsten with fluorine.[187] Note that the stable solid by-products at room temperature tend to be redeposited on other surfaces. Ion-assisted reactions have solved the redeposition problem. The etching of metals also has the problem of the redeposition of etching by-products.[12,188–197]

In self-limiting formation, another difficulty arises for intermetallic compounds or alloys such as CoFe, NiFe, CrFe, and PtMn. Simply, in etching processes for compounds such as high-k materials, dichalcogenides, GaAs, GaP, and GaN, it is difficult to maintain the surface stoichiometry during and after the etching. The stoichiometric changes arise from differences in the volatilities of the etching by-products. For example, here are different vapor pressures for metal chlorides such as $AlCl_3$, $GaCl_3$, and NCl_3 in AlGaN etching at temperatures around room temperature. Since the vapor pressures depend on temperature, the etching reaction temperatures should be taken into consideration. The volatilities of etching by-products in the GaN etching processes have been discussed in terms of surface roughness.[198–201] Self-limiting chlorination and removal of the modified layer by ion irradiation have been utilized. Ohba et al. reported the formation of surface roughness on AlGaN in cyclic etching involving Cl_2 plasma exposure and Ar ion bombardment.[202] We point out that the atomic-level-control of surface reactions will be required for the etching of intermetallic compounds and alloys.

Additional examples of directional ALEt with ion bombardment are the self-limiting deposition of thin fluorocarbon film and their removal with ion bombardment. The

fluorocarbon film thickness depends on the underlying surface material. For example, thinner films were deposited and higher etching rates were observed for silicon oxides and nitrides, while thicker films and lower etching rates were observed for silicon surfaces.[203,204]

For the case of metal ALEt, low energy ion bombardment is useful in the self-limiting formation of a ligand-exchange layer. In Fig. 11, the ion bombardment may play two roles in ALEt. One is the removal of products in the self-limiting modified layer. The other is the pretreatment in which an active surface is formed in a self-limiting manner on the surface. The active surface provides high reactivity with reactants to form the modified layer because the isolated metal atoms may enable ligand coordination, allowing chelating products centered around the metal atom to be used for etching. The development of revolutionary methods is needed to meet the challenges described in this section.

5. Conclusions

We have discussed the advances in fabrication technologies in atomic layer processing for emerging materials and the state-of-the-art in plasma etching for industrial applications to semiconductors. We reviewed atomic layer processing from the perspective of physicochemical reactions and equipment parameter control in terms of ion trajectories and gas-flow velocity distributions in reactor chambers. The reviewed matter includes an outline of major challenges in future research on the atomic layer fidelity of dry processes. We have addressed parameters related to the discharge species and wafer temperature that should be diagnosed using real-time in situ methods since dry etching processes exist in states of dynamic equilibrium. The major challenges must be addressed using complementary experimental and computational approaches.

Acknowledgements

The authors would like to thank Drs. Masanobu Honda, Miyako Matsui, Tomohiro Okumura, Tetsuya Tatsumi, Satoshi Hamaguchi, Hiroto Ohtake, Yoshinobu Ohya, Kazunori Shinoda, Masaru Izawa, Hisataka Hayashi, Toshio Hayashi, Makoto Sekine, and Masaru Hori, and all members of the Program and Publication Committee of the 38th International Symposium on Dry Process 2016 held in Sapporo, Japan, as well as Nicholas Altieri and Jeffrey Chang at UCLA for proofreading and providing feedback on the manuscript.

1) N. Hosokawa, R. Matsuzaki, and T. Asamaki, Jpn. J. Appl. Phys. **13**, 435 (1974).
2) H. Abe, M. Yoneda, and N. Fujiwara, Jpn. J. Appl. Phys. **47**, 1435 (2008).
3) M. Lieberman and A. J. Lichtenberg, *Principles of Plasma Discharges and Materials Processing* (Wiley, New York, 2005) 2nd ed.
4) P. Charbert and N. Braithwaite, *Physics of Radio-Frequency Plasmas* (Cambridge University Press, Cambridge, U.K., 2012).
5) K. Nojiri, *Dry Etching Technology for Semiconductors* (Springer, Heidelberg, 2015).
6) M. Sekine, Appl. Surf. Sci. **192**, 270 (2002).
7) T. Tatsumi, M. Matsui, M. Okigawa, and M. Sekine, J. Vac. Sci. Technol. B **18**, 1897 (2000).
8) M. M. Waldrop, Nature **530**, 144 (2016).
9) 2015 International Roadmap for Semiconductors (ITRS) 2.0.
10) H. Tanaka, M. Kido, K. Yahashi, M. Oomura, R. Katsumata, M. Kito, Y. Fukuzumi, M. Sato, Y. Nagata, Y. Matsuoka, Y. Iwata, H. Aochi, and A. Nitayama, Proc. VLSI Tech. Dig., 2007, p. 14.
11) K. Eriguchi, Jpn. J. Appl. Phys. **56**, 06HA01 (2017).
12) H. Ohtake, S. Samukawa, H. Oikawa, and Y. Nashimoto, Jpn. J. Appl. Phys. **37**, 2311 (1998).
13) T. Faraz, F. Roozeboom, H. C. M. Knoops, and W. M. M. Kessels, ECS J. Solid State Sci. Technol. **4**, N5023 (2015).
14) K. J. Kanarik, T. Lill, E. A. Hudson, S. Sriraman, S. Tan, J. Marks, V. Vahedi, and R. A. Gottscho, J. Vac. Sci. Technol. A **33**, 020802 (2015).
15) Y. Horiike, T. Tanaka, M. Nakano, S. Iseda, H. Sakaue, A. Nagata, H. Shindo, S. Miyazaki, and M. Hirose, J. Vac. Sci. Technol. A **8**, 1844 (1990).
16) H. Sakaue, S. Iseda, K. Asami, J. Yamamoto, M. Hirose, and Y. Horiike, Jpn. J. Appl. Phys. **29**, 2648 (1990).
17) Y. Morikawa, K. Kubota, H. Ogawa, T. Ichiki, A. Tachibana, S. Fujimura, and Y. Horiike, J. Vac. Sci. Technol. A **16**, 345 (1998).
18) H. Nishino, N. Hayasaka, and H. Okano, J. Appl. Phys. **74**, 1345 (1993).
19) J. Kikuchi, S. Fujimura, M. Suzuki, and H. Yano, Jpn. J. Appl. Phys. **32**, 3120 (1993).
20) J. Kikuchi, M. Iga, H. Ogawa, S. Fujimura, and H. Yano, Jpn. J. Appl. Phys. **33**, 2207 (1994).
21) J. Kikuchi, M. Nagasaka, S. Fujimura, and H. Yano, Jpn. J. Appl. Phys. **35**, 1022 (1996).
22) M. T. Suzuki, J. Kikuchi, M. Nagasaka, and S. Fujimura, MRS Proc. **477**, 167 (1997).
23) H. Ogawa, T. Arai, M. Yanagisawa, T. Ichiki, and Y. Horiike, Jpn. J. Appl. Phys. **41**, 5349 (2002).
24) T. Hayashi, K. Ishikawa, M. Sekine, M. Hori, A. Kono, and K. Suu, Jpn. J. Appl. Phys. **51**, 016201 (2012).
25) T. Hayashi, K. Ishikawa, M. Sekine, M. Hori, A. Kono, and K. Suu, Jpn. J. Appl. Phys. **51**, 026505 (2012).
26) T. Hayashi, J. Nanomed. Nanotechnol. **S15**, 1 (2013).
27) N. Posseme, A. Ah-Leung, O. Pollet, C. Arvet, and M. Garcia-Barros, J. Vac. Sci. Technol. A **34**, 061301 (2016).
28) T. S. Cho, Q. Han, D. Yang, S. Park, D. Lubomirsky, and S. Venkataraman, Jpn. J. Appl. Phys. **55**, 056201 (2016).
29) W. C. Natzle, D. Horak, S. Deshpande, C.-F. Yu, J. C. Liu, R. W. Mann, B. Doris, H. Hanafi, J. Brown, A. Sekiguchi, M. Tomoyasu, A. Yamashita, D. Prager, M. Funk, P. Cottrell, F. Higuchi, H. Takahashi, M. Sendelbach, E. Solecky, W. Yan, L. Tsou, Q. Yang, J. P. Norum, and S. S. Iyer, Proc. IEEE Advanced Semiconductor Manufacturing Conf. (ASMC '04), 2004, p. 61.
30) K. Tapily, S. Consiglio, R. D. Clark, R. Vasic, C. S. Wajda, J. Jordan-Sweet, G. J. Leusink, and A. C. Diebold, ECS J. Solid State Sci. Technol. **4**, N1 (2015).
31) J. Lei, S.-E. Phan, X. Lu, C.-T. Kao, K. Lavu, K. Moraes, K. Tanaka, B. Wood, B. Ninan, and S. Gandikota, Proc. IEEE Int. Symp. Semiconductor Manufacturing (ISSM 2006), 2006, p. 393.
32) R. Yang, N. Su, P. Bonfanti, J. Nie, J. Ning, and T. T. Li, J. Vac. Sci. Technol. B **28**, 56 (2010).
33) K.-F. Lo, F.-H. Hsu, X.-G. Lin, H.-J. Lee, N.-T. Lian, T. Yang, and K.-C. Chen, Proc. IEEE Advanced Semiconductor Manufacturing Conf. (ASMC '15), 2015, p. 309.
34) K. Shinoda, M. Izawa, T. Kanekiyo, K. Ishikawa, and M. Hori, Appl. Phys. Express **9**, 106201 (2016).
35) K. Shinoda, N. Miyoshi, H. Kobayashi, M. Miura, M. Kurihara, K. Maeda, N. Negishi, Y. Sonoda, M. Tanaka, N. Yasui, M. Izawa, Y. Ishii, K. Okuma, T. Saldana, J. Manos, K. Ishikawa, and M. Hori, J. Phys. D **50**, 016201 (2012).
36) N. Miyoshi, H. Kobayashi, K. Shinoda, M. Kurihara, T. Watanabe, Y. Kouzuma, K. Yokogawa, S. Sakai, and M. Izawa, Jpn. J. Appl. Phys. **56**, 06HB01 (2017).
37) A. Ludviksson, M. Xu, and R. M. Mratin, Surf. Sci. **277**, 282 (1992).
38) T. Meguro, M. Hamagaki, S. Modaressi, T. Hara, Y. Aoyagi, M. Ishii, and Y. Yamamoto, Appl. Phys. Lett. **56**, 1552 (1990).
39) Y. Aoyagi, K. Shinmura, K. Kawasaki, T. Tanaka, K. Gamo, S. Namba, and I. Nakamoto, Appl. Phys. Lett. **60**, 968 (1992).
40) M. Ishii, T. Meguro, H. Kodama, Y. Yamamoto, and Y. Aoyagi, Jpn. J. Appl. Phys. **31**, 2212 (1992).
41) T. Meguro, M. Ishii, K. Kodama, Y. Yamamoto, K. Gamo, and Y. Aoyagi, Thin Solid Films **225**, 136 (1993).
42) M. Ishii, T. Meguro, K. Gamo, T. Sugano, and Y. Aoyagi, Jpn. J. Appl. Phys. **32**, 6178 (1993).
43) T. Meguro, M. Ishii, T. Sugano, K. Gamo, and Y. Aoyagi, Appl. Surf. Sci. **82–83**, 193 (1994).
44) T. Matsuura, H. Uetake, T. Ohmi, J. Murota, K. Fukuda, N. Mikoshiba, T. Kawashima, and Y. Yamashita, Appl. Phys. Lett. **56**, 1339 (1990).
45) T. Matsuura, J. Murota, Y. Sawada, and T. Ohmi, Appl. Phys. Lett. **63**,

2803 (1993).
46) T. Sugiyama, T. Matsuura, and J. Murota, Appl. Surf. Sci. **112**, 187 (1997).
47) T. Matsuura, Y. Honda, and J. Murota, Appl. Phys. Lett. **74**, 3573 (1999).
48) B. Degroote, R. Rooyackers, T. Vandeweyer, N. Collaert, W. Boullart, E. Kunnen, D. Shamiryan, J. Wouters, J. Van Puymbroeck, A. Dixit, and M. Jurczak, Microelectron. Eng. **84**, 609 (2007).
49) A. J. M. Mackus, A. A. Bol, and W. M. M. Kessels, Nanoscale **6**, 10941 (2014).
50) S. E. Potts, W. Keuning, E. Langereis, G. Dingemans, M. C. M. van de Sanden, and W. M. M. Kessels, J. Electrochem. Soc. **157**, P66 (2010).
51) S. E. Potts, H. B. Profijt, R. Roelofs, and W. M. M. Kessels, Chem. Vapor Deposition **19**, 125 (2013).
52) S. B. S. Heil, E. Langereis, F. Roozeboom, M. C. M. van de Sanden, and W. M. M. Kessels, J. Electrochem. Soc. **153**, G956 (2006).
53) E. Langereis, H. C. M. Knoops, A. J. M. Mackus, F. Roozeboom, M. C. M. van de Sanden, and W. M. M. Kessels, J. Appl. Phys. **102**, 083517 (2007).
54) H. C. M. Knoops, E. M. J. Braeken, K. de Peuter, S. E. Potts, S. Haukka, V. Pore, and W. M. M. Kessels, ACS Appl. Mater. Interfaces **7**, 19857 (2015).
55) H. C. M. Knoops, K. de Peuter, and W. M. M. Kessels, Appl. Phys. Lett. **107**, 014102 (2015).
56) Y. Lu, A. Kobayashi, H. Kondo, K. Ishikawa, M. Sekine, and M. Hori, Jpn. J. Appl. Phys. **53**, 010305 (2014).
57) A. J. M. Mackus, D. Garcia-Alonso, H. C. M. Knoops, A. A. Bol, and W. M. M. Kessels, Chem. Mater. **25**, 1769 (2013).
58) M. J. Weber, A. J. M. Mackus, M. A. Verheijen, V. Longo, A. A. Bol, and W. M. M. Kessels, J. Phys. Chem. C **118**, 8702 (2014).
59) H. B. Profijt, S. E. Potts, M. C. M. van de Sanden, and W. M. M. Kessels, J. Vac. Sci. Technol. A **29**, 050801 (2011).
60) F. Koehler, D. H. Triyoso, I. Hussain, B. Antonioli, and K. Hempel, Phys. Status Solidi C **11**, 73 (2014).
61) C. K. Ande, H. C. M. Knoops, K. de Peuter, M. van Drunen, S. D. Elliott, and W. M. M. Kessels, J. Phys. Chem. Lett. **6**, 3610 (2015).
62) H. B. Profijt, P. Kudlacek, M. C. M. van de Sanden, and W. M. M. Kessels, J. Electrochem. Soc. **158**, G88 (2011).
63) H. B. Profijt, M. C. M. van de Sanden, and W. M. M. Kessels, Electrochem. Solid-State Lett. **15**, G1 (2012).
64) H. B. Profijt, M. C. M. van de Sanden, and W. M. M. Kessels, J. Vac. Sci. Technol. A **31**, 01A106 (2013).
65) K. K. Ko and S. W. Pang, J. Vac. Sci. Technol. B **11**, 2275 (1993).
66) S. D. Athavale and D. J. Economou, J. Vac. Sci. Technol. B **14**, 3702 (1996).
67) B. J. Kim, S. H. Chung, and S. M. Cho, Appl. Surf. Sci. **187**, 124 (2002).
68) A. Agarwal and M. J. Kushner, J. Vac. Sci. Technol. A **27**, 37 (2009).
69) T. Lin, B. Kang, M. Jeon, C. Huffman, J. Jeon, S. Lee, W. Han, J. Lee, S. Lee, and G. Y. Yeom, ACS Appl. Mater. Interfaces **7**, 15892 (2015).
70) H. Zhu, X. Y. Ain, L. X. Cheng, A. Azcatl, J. Kim, and R. M. Wallace, ACS Appl. Mater. Interfaces **8**, 19119 (2016).
71) W. S. Lim, Y. Y. Kim, H. Kim, S. Jang, N. Kwon, B. J. Park, J. H. Ahn, I. Chung, B. H. Hong, and G. Y. Yeom, Carbon **50**, 429 (2012).
72) D. Metzler, R. L. Bruce, S. Engelmann, E. A. Joseph, and G. S. Oehrlein, J. Vac. Sci. Technol. A **32**, 020603 (2014).
73) D. Metzler, C. Li, S. Engelmann, R. L. Bruce, E. A. Joseph, and G. S. Oehrlein, J. Vac. Sci. Technol. A **34**, 01B101 (2016).
74) N. Posseme, O. Pollet, and B. S. Barnola, Appl. Phys. Lett. **105**, 051605 (2014).
75) Y. Lee and S. M. George, ACS Nano **9**, 2061 (2015).
76) Y. Lee, J. W. DuMont, and S. M. George, Chem. Mater. **27**, 3648 (2015).
77) Y. Lee, J. W. DuMont, and S. M. George, ECS J. Solid State Sci. Technol. **4**, N5013 (2015).
78) Y. Lee, J. W. DuMont, and S. M. George, Chem. Mater. **28**, 2994 (2016).
79) S. M. George and Y. Lee, ACS Nano **10**, 4889 (2016).
80) N. R. Johnson, H. Sun, K. Sharma, and S. M. George, J. Vac. Sci. Technol. A **34**, 050603 (2016).
81) D. R. Zywotko and S. M. George, Chem. Mater. **29**, 1183 (2017).
82) J. W. DuMont, A. E. Marquardt, A. M. Cano, and S. M. George, ACS Appl. Mater. Interfaces **9**, 10296 (2017).
83) K. L. Wang and P. K. Amiri, Spin **2**, 1250009 (2012).
84) C. D. Pham, J. Chang, M. A. Zurbuchen, and J. P. Chang, Chem. Mater. **27**, 7282 (2015).
85) J. Chang and J. P. Chang, to be published in J. Phys. D: Appl. Phys. (2017).
86) D. Chien, X. Li, K. Wong, M. A. Zurbuchen, S. Robbennolt, G. Yu, S. Tolbert, N. Kioussis, P. K. Amiri, K. L. Wang, and J. P. Chang, Appl. Phys. Lett. **108**, 112402 (2016).
87) X. Li, K. Fitzell, D. Wu, C. T. Karaba, A. Buditama, G. Yu, K. L. Wong, N. Altieri, C. Grezes, N. Kioussis, S. Tolbert, Z. Zhang, J. P. Chang, P. K. Amiri, and K. L. Wang, Appl. Phys. Lett. **110**, 052401 (2017).
88) K. Kinoshita, H. Utsumi, K. Suemitsu, H. Hada, and T. Sugibayashi, Jpn. J. Appl. Phys. **49**, 08JB02 (2010).
89) K. Kinoshita, H. Honjo, S. Fukami, H. Sato, K. Mizunuma, K. Tokutome, M. Murahata, S. Ikeda, S. Miura, N. Kasai, and H. Ohno, Jpn. J. Appl. Phys. **53**, 103001 (2014).
90) K. Kinoshita, T. Yamamoto, H. Honjo, N. Kasai, S. Ikeda, and H. Ohno, Jpn. J. Appl. Phys. **51**, 08HA01 (2012).
91) K. Kinoshita, H. Honjo, S. Fukami, R. Nebashi, K. Tokutome, M. Murahata, S. Miura, N. Kasai, S. Ikeda, and H. Ohno, Jpn. J. Appl. Phys. **53**, 03DF03 (2014).
92) T. Kim, J. K.-C. Chen, and J. P. Chang, J. Vac. Sci. Technol. A **32**, 041305 (2014).
93) T. Kim, Y. Kim, J. K.-C. Chen, and J. P. Chang, J. Vac. Sci. Technol. A **33**, 021308 (2015).
94) J. K.-C. Chen, T. Kim, N. D. Altieri, E. Chen, and J. P. Chang, J. Vac. Sci. Technol. A **35**, 031304 (2017).
95) J. K.-C. Chen, N. D. Altieri, T. Kim, T. Lill, M. Shen, and J. P. Chang, J. Vac. Sci. Technol. A **35**, 05C304 (2017).
96) J. K.-C. Chen, N. D. Altieri, T. Kim, E. Chen, T. Lill, M. Shen, and J. P. Chang, J. Vac. Sci. Technol. A **35**, 05C305 (2017).
97) J. K.-C. Chen, T. Kim, and J. P. Chang, ECS Trans. **75** [33], 1 (2017).
98) D. Chien, A. N. Buditama, L. T. Schelhas, H. Y. Kang, S. Robbennolt, J. P. Chang, and S. H. Tolbert, Appl. Phys. Lett. **109**, 112904 (2016).
99) S. Jesse, A. Y. Borisevich, J. D. Fowlkes, A. R. Lupini, P. D. Rack, R. R. Unocic, B. G. Sumpter, S. V. Kalinin, A. Belianinov, and O. S. Ovchinnikova, ACS Nano **10**, 5600 (2016).
100) F. A. Stevie, L. Giannuzzi, and B. Prenitzer, *The Focused Ion Beam Instrument. Introduction to Focused Ion Beams* (Springer, Heidelberg, 2005) p. 1.
101) J. Gierak, A. Septier, and C. Vieu, Nucl. Instrum. Methods Phys. Res., Sect. A **427**, 91 (1999).
102) N. P. Economou, J. A. Notte, and W. B. Thompson, Scanning **34**, 83 (2012).
103) B. Ward, J. A. Notte, and N. Economou, J. Vac. Sci. Technol. B **24**, 2871 (2006).
104) F. Rahman, S. McVey, L. Farkas, J. A. Notte, S. Tan, and R. H. Livengood, Scanning **34**, 129 (2012).
105) N. F. W. Thissen, R. J. H. Vervuurt, A. C. M. Mackus, J. L. L. Mulders, J. W. Weber, W. M. M. Kessels, and A. A. Bol, 2D Mater. **4**, 025046 (2017).
106) S. Hwang and K. Kanarik, Solid State Technol. **59** [5], 16 (2016).
107) N. Y. Babaeva and M. J. Kushner, J. Phys. D **41**, 062004 (2008).
108) K. Maeda, K. Yokogawa, T. Ichino, T. Tamura, K. Hirozane, T. Kanekiyo, and M. Izawa, Proc. 31st Int. Symp. Dry Process, 2009, p. 257.
109) T. Kubota, H. Ohtake, R. Araki, Y. Yanagisawa, T. Iwasaki, K. Ono, K. Miwa, and S. Samukawa, J. Phys. D **46**, 415203 (2013).
110) K. Denpoh, Jpn. J. Appl. Phys. **53**, 080304 (2014).
111) J. H. Um, T. K. Kang, H.-J. Park, and T.-Y. Yoon, Proc. 38th Int. Symp. Dry Process, 2016, F-2, p. 181.
112) S. Tachi, K. Tsujimoto, and S. Okudaira, Appl. Phys. Lett. **52**, 616 (1988).
113) J. Pelletier, Appl. Phys. Lett. **53**, 1665 (1988).
114) S. Tachi, K. Tsujimoto, and S. Okudaira, Appl. Phys. Lett. **53**, 1666 (1988).
115) T. D. Bestwick, G. S. Oehrlein, and D. Angell, Appl. Phys. Lett. **57**, 431 (1990).
116) T. Mizutani, T. Yunogami, and T. Tsujimoto, Appl. Phys. Lett. **57**, 1654 (1990).
117) W. Varhue, J. Burroughs, and W. Mlynko, J. Appl. Phys. **72**, 3050 (1992).
118) M. Hara, T. Masuzumi, Z. Lu, C. Kimura, H. Aoki, and T. Sugino, Jpn. J. Appl. Phys. **49**, 04DB10 (2010).
119) B. Wu, A. Kumar, and S. Pamarthy, J. Appl. Phys. **108**, 051101 (2010).
120) T. Seki, Y. Yoshino, T. Senoo, K. Koike, T. Aoki, and J. Matsuo, Jpn. J. Appl. Phys. **55**, 06HB01 (2016).
121) T. Seki, H. Yamamoto, T. Kozawa, T. Shojo, K. Koike, T. Aoki, and J. Matsuo, Jpn. J. Appl. Phys. **56**, 06HB02 (2017).
122) K. Nakamatsu, M. Okada, and S. Matsui, Jpn. J. Appl. Phys. **47**, 8619 (2008).
123) C.-L. Wu, M.-C. Yip, and W. Fang, Jpn. J. Appl. Phys. **48**, 06FK06 (2009).
124) J. Han, T.-G. Kim, B.-K. Min, and S. J. Lee, Jpn. J. Appl. Phys. **49**, 06GK04 (2010).
125) H. Miyashita, E. Tomono, Y. Kawai, M. Toda, M. Esashi, and T. Ono, Jpn. J. Appl. Phys. **50**, 106503 (2011).
126) S. Tajima, T. Hayashi, K. Ishikawa, M. Sekine, and M. Hori, J. Phys. Chem. C **117**, 5118 (2013).

127) S. Tajima, T. Hayashi, K. Ishikawa, M. Sekine, and M. Hori, J. Phys. Chem. C **117**, 20810 (2013).
128) X. Mellhaoui, R. Dussart, T. Tillocher, P. Lefaucheux, P. Ranson, M. Boufnichel, and L. J. Overzet, J. Appl. Phys. **98**, 104901 (2005).
129) J. Pereira, L. E. Pichon, R. Dussart, C. Cardinaud, C. Y. Duluard, E. H. Oubensaid, P. Lefaucheux, M. Boufnichel, and P. Ranson, Appl. Phys. Lett. **94**, 071501 (2009).
130) V. Ishchuk, D. L. Olynick, Z. Liu, and I. W. Rangelow, J. Appl. Phys. **118**, 053302 (2015).
131) R. Dussart, T. Tillocher, P. Lefaucheux, and M. Boufinichel, J. Phys. D **47**, 123001 (2014).
132) M. J. Kushner, J. Phys. D **42**, 194013 (2009).
133) S. Tinck, T. Tillocher, R. Dussart, and A. Bogaerts, J. Phys. D **48**, 155204 (2015).
134) S. Tinck, E. Neyts, and A. Bogaerts, J. Phys. Chem. C **118**, 30315 (2014).
135) C. K. Birdall and A. B. Langdon, *Plasma Physics via Computer Simulation* (McGraw-Hill, New York, 1985).
136) L. L. Raja, S. Mahadevan, P. L. G. Ventzek, and J. Yoshikawa, J. Vac. Sci. Technol. A **31**, 031304 (2013).
137) K. Miyake, T. Ito, M. Isobe, K. Karahashi, M. Fukasawa, K. Nagahata, T. Tatsumi, and S. Hamaguchi, Jpn. J. Appl. Phys. **53**, 03DD02 (2014).
138) N. Nakazaki, Y. Takao, K. Eriguchi, and K. Ono, Jpn. J. Appl. Phys. **53**, 056201 (2014).
139) T. Shimada, T. Yagisawa, and T. Makabe, Jpn. J. Appl. Phys. **45**, L132 (2006).
140) S. Takagi, S. Onoue, K. Nishitani, T. Shinnmura, and Y. Shigesato, Jpn. J. Appl. Phys. **54**, 036501 (2015).
141) N. Kuboi, M. Fukasawa, and T. Tatsumi, Jpn. J. Appl. Phys. **55**, 07LA02 (2016).
142) V. Vahedi and M. Surendra, Comput. Phys. Commun. **87**, 179 (1995).
143) H. J. Kim and H. J. Lee, Plasma Sources Sci. Technol. **25**, 035006 (2016).
144) H. J. Kim and H. J. Lee, Plasma Sources Sci. Technol. **25**, 065006 (2016).
145) Y. Zhang and M. J. Kushner, J. Vac. Sci. Technol. A **33**, 031302 (2015).
146) M. G. Lagally, Jpn. J. Appl. Phys. **32**, 1493 (1993).
147) K. Ishikawa, K. Karahashi, H. Tsuboi, K. Yanai, and M. Nakamura, J. Vac. Sci. Technol. A **21**, L1 (2003).
148) K. Yanai, K. Karahashi, K. Ishikawa, and M. Nakamura, J. Appl. Phys. **97**, 053302 (2005).
149) T. Ito, K. Karahashi, M. Fukasawa, T. Tatsumi, and S. Hamaguchi, J. Vac. Sci. Technol. A **29**, 050601 (2011).
150) K. Karahashi, H. Li, K. Yamada, T. Ito, S. Numazawa, K. Machida, K. Ishikawa, and S. Hamaguchi, Jpn. J. Appl. Phys. **56**, 06HB09 (2017).
151) V. M. Donnelly and J. A. McCaulley, J. Vac. Sci. Technol. A **8**, 84 (1990).
152) V. M. Donnelly, J. Vac. Sci. Technol. A **11**, 2393 (1993).
153) K. Takeda, Y. Tomekawa, T. Shiina, M. Ito, Y. Okamura, and N. Ishii, Jpn. J. Appl. Phys. **43**, 7737 (2004).
154) C. Koshimizu, T. Ohta, T. Matsudo, S. Tsuchitani, and M. Ito, Jpn. J. Appl. Phys. **51**, 046201 (2012).
155) T. Tsutsumi, K. Ishikawa, K. Takeda, H. Kondo, T. Ohta, M. Ito, M. Sekine, and M. Hori, Jpn. J. Appl. Phys. **55**, 01AB04 (2016).
156) K. Ohno and M. Sato, Jpn. J. Appl. Phys. **28**, L1070 (1989).
157) G. Levitin and D. W. Hess, Annu. Rev. Chem. Biomol. Eng. **2**, 299 (2011).
158) R. Steger and R. Masel, Thin Solid Films **342**, 221 (1999).
159) M. A. George, D. W. Hess, S. E. Beck, J. C. Ivankovits, D. A. Bohling, and A. P. Lane, J. Electrochem. Soc. **142**, 961 (1995).
160) K. Ueno, V. M. Donnelly, and K. Kikkawa, J. Electrochem. Soc. **144**, 2565 (1997).
161) K. Ueno, V. M. Donnelly, Y. Tsuchiya, and H. Aoki, MRS Proc. **564**, 521 (1999).
162) K. L. Chavez and D. W. Hess, J. Electrochem. Soc. **148**, G640 (2001).
163) K. Ishikawa, T. Yagishita, and M. Nakamura, MRS Proc. **766**, E3.28 (2003).
164) T. Yaghishita, K. Ishikawa, and M. Nakamura, Proc. Electrochem. Soc. **13**, 320 (2003).
165) W. Yang, M. Akaike, M. Fujino, and T. Suga, ECS J. Solid State Sci. Technol. **2**, P271 (2013).
166) J.-M. Song, S.-K. Huang, M. Akaike, and T. Suga, Jpn. J. Appl. Phys. **54**, 030217 (2015).
167) N. S. Kulkarni, P. Tamirisa, G. Levitin, R. Kasica, and D. W. Hess, MRS Proc. **914**, 0914-F09-08 (2006).
168) P. A. Tamirisa, G. Levitin, N. S. Kulkarni, and D. W. Hess, Microelectron. Eng. **84**, 105 (2007).
169) F. Wu, G. Levitin, and D. W. Hess, J. Electrochem. Soc. **157**, H474 (2010).
170) F. Wu, G. Levitin, and D. Hess, ECS Trans. **33** [12], 157 (2010).
171) F. Wu, G. Levitin, and D. W. Hess, ACS Appl. Mater. Interfaces **2**, 2175 (2010).
172) F. Wu, G. Levitin, and D. W. Hess, J. Vac. Sci. Technol. B **29**, 011013 (2011).
173) F. Wu, G. Levitin, and D. W. Hess, J. Electrochem. Soc. **159**, H121 (2012).
174) F. Wu, G. Levitin, T.-S. Choi, and D. W. Hess, ECS Trans. **44** [1], 299 (2012).
175) T.-S. Choi, G. Levitin, and D. W. Hess, ECS J. Solid State Sci. Technol. **2**, P275 (2013).
176) T.-S. Choi, G. Levitin, and D. W. Hess, ECS J. Solid State Sci. Technol. **2**, P506 (2013).
177) T. S. Choi and D. W. Hess, J. Vac. Sci. Technol. B **33**, 012202 (2015).
178) D. W. Hess, ECS Trans. **61** [3], 91 (2014).
179) T. S. Choi and D. W. Hess, ECS J. Solid State Sci. Technol. **4**, N3084 (2015).
180) A. A. Garay, J. H. Choi, S. M. Hwang, and C. W. Chung, ECS Solid State Lett. **4**, P77 (2015).
181) T. Suda, N. Toyoda, K. Hara, and I. Yamada, Jpn. J. Appl. Phys. **51**, 08HA02 (2012).
182) A. Yamaguchi, R. Hinoura, N. Toyoda, K. Hara, and I. Yamada, Jpn. J. Appl. Phys. **52**, 05EB05 (2013).
183) N. Toyoda, A. Fujimoto, and I. Yamada, Jpn. J. Appl. Phys. **52**, 06GF01 (2013).
184) R. Hinoura, A. Yamaguchi, N. Toyoda, K. Hara, and I. Yamada, Jpn. J. Appl. Phys. **53**, 03DD05 (2014).
185) N. Toyoda, K. Sumie, A. Kimura, and I. Yamada, Jpn. J. Appl. Phys. **53**, 05FC01 (2014).
186) S. U. Engelmann, R. L. Bruce, M. Nakamura, D. Metzler, S. G. Walton, and E. A. Joseph, ECS J. Solid State Sci. Technol. **4**, N5054 (2015).
187) N. Kofuji, M. Mori, and T. Nishida, Jpn. J. Appl. Phys. **56**, 06HB05 (2017).
188) S. Samukawa, S. Kumagai, and T. Shiraiwa, Jpn. J. Appl. Phys. **42**, L1272 (2003).
189) T. Mukai, H. Hada, S. Tahara, H. Yoda, and S. Samukawa, Jpn. J. Appl. Phys. **45**, 5542 (2006).
190) T. Mukai, H. Hada, S. Tahara, H. Yoda, and S. Samukawa, J. Vac. Sci. Technol. A **25**, 432 (2007).
191) S. Noda, T. Ozaki, and S. Samukawa, J. Vac. Sci. Technol. A **24**, 1414 (2006).
192) S. W. Chun, D. H. Kim, J. H. Kwon, B. H. Kim, S. J. Choi, and S. B. Lee, J. Appl. Phys. **111**, 07C722 (2012).
193) M. H. Jeon, H. J. Kim, K. C. Yang, S. K. Kang, K. N. Kim, and G. Y. Yeom, Jpn. J. Appl. Phys. **52**, 05EB03 (2013).
194) M. H. Jeon, K. C. Yang, J. W. Park, D. H. Yun, K. N. Kim, and G. Y. Yeom, J. Nanosci. Nanotechnol. **16**, 11823 (2016).
195) H. Li, Y. Muraki, K. Karahashi, and S. Hamaguchi, J. Vac. Sci. Technol. A **33**, 040602 (2015).
196) M. Satake, M. Yamada, H. Li, K. Karahashi, and S. Hamaguchi, J. Vac. Sci. Technol. B **33**, 051810 (2015).
197) M. Satake, M. Yamada, and E. Matsumoto, J. Vac. Sci. Technol. **34**, 061806 (2016).
198) R. Kometani, K. Ishikawa, K. Takeda, H. Kondo, M. Sekine, and M. Hori, Appl. Phys. Express **6**, 056201 (2013).
199) R. Kometani, K. Ishikawa, K. Takeda, H. Kondo, M. Sekine, and M. Hori, Trans. Mater. Res. Soc. Jpn. **38**, 325 (2013).
200) Z. Liu, J. Pan, T. Kako, K. Ishikawa, O. Oda, K. Takeda, H. Kondo, M. Sekine, and M. Hori, Jpn. J. Appl. Phys. **54**, 06GB04 (2015).
201) Z. Liu, J. Pan, A. Asano, K. Ishikawa, K. Takeda, H. Kondo, O. Oda, M. Sekine, and M. Hori, Jpn. J. Appl. Phys. **56**, 026502 (2017).
202) T. Ohba, W. Yang, S. Tan, K. J. Kanarik, and K. Nojiri, Jpn. J. Appl. Phys. **56**, 06HB06 (2017).
203) Y. Ishii, K. Okuma, T. Saldana, K. Maeda, N. Negishi, and J. Manos, Jpn. J. Appl. Phys. **56**, 06HB07 (2017).
204) M. Tabata, A. Tsuji, T. Katsunuma, and M. Honda, Jpn. J. Appl. Phys. **56**, 06HB08 (2017).